Shock Waves (2011) 21:1–17
DOI 10.1007/s00193-010-0282-y

ORIGINAL ARTICLE

Effect of wall heat transfer on shock-tube test temperature at long times

C. Frazier · M. Lamnaouer · E. Divo · A. Kassab · E. Petersen

Received: 30 September 2009 / Revised: 1 February 2010 / Accepted: 6 September 2010 / Published online: 9 October 2010

Abstract When performing chemical kinetics experiments behind reflected shock waves at conditions of lower temperature (<1,000 K), longer test times on the order of 10–20 ms may be required. The integrity of the test temperature during such experiments may be in question, because heat loss to the tube walls may play a larger role than is generally seen in shock-tube kinetics experiments that are over within a millisecond or two. A series of detailed calculations was performed to estimate the effect of longer test times on the temperature uniformity of the post-shock test gas. Assuming the main mode of heat transfer is conduction between the high-temperature gas and the colder shock-tube walls, a comprehensive set of calculations covering a range of conditions including test temperatures between 800 and 1,800 K, pressures between 1 and 50 atm, driven-tube inner diameters between 3 and 16.2 cm, and test gases of N_2 and Ar was performed. Based on the results, heat loss to the tube walls does not significantly reduce the area-averaged temperature behind the reflected shock wave for test conditions that are likely to be used in shock-tube studies for test times up to 20 ms (and higher), provided the shock-tube inner diameter is sufficiently large (>8 cm). Smaller diameters on the order of 3 cm or less can experience significant temperature loss near the reflected-shock region. Although the area-averaged gas temperature decreases due to the heat loss, the main core region remains spatially uniform so that the zone of temperature change is limited to only the thermal layer adjacent to the walls. Although the heat conduction model assumes the gas and wall to behave as solid bodies, resulting in a core gas temperature that remains constant at the initial temperature, a two-zone gas model that accounts for density loss from the core to the colder thermal layer indicates that the core temperature and gas pressure both decrease slightly with time. A full CFD solution of the shock-tube flow field and heat transfer at long test times was also performed for one typical condition (800 K, 1 atm, Ar), the results of which indicate that the simpler analytical conduction model is realistic but somewhat conservative in that it over predicts the mean temperature loss by a few Kelvins. This paper presents the first comprehensive study on the effects of long test times on the average test gas temperature behind the reflected shock wave for conditions representative of chemical kinetics experiments.

Keywords Shock tube · Heat transfer · Chemical kinetics · Driver gas tailoring · CFD

Communicated by R. Hanson.

A part of this paper is based on work that was presented at the 26th International Symposium on Shock Waves, Goettingen, Germany, 15–20 July 2007.

C. Frazier · E. Petersen (✉)
Department of Mechanical Engineering, Texas A&M University, College Station, TX, USA
e-mail: epetersen@tamu.edu

M. Lamnaouer · E. Divo · A. Kassab
Mechanical, Materials and Aerospace Engineering, University of Central Florida, Orlando, FL, USA

1 Introduction

Shock-tube experiments have traditionally been performed at short test times (around 1 ms) with the assumption that such a short test time allows the region behind the reflected shock wave to be considered isothermal. Often, high test temperatures greater than about 1,400 K are used to ensure chemical reaction occurs within these short test times and maintain thermal integrity, as lower test temperatures would slow down the chemistry; the longer test times could result

in greater heat loss from the test gas. Reflected shock waves allow researchers to create controllable, high-temperature and pressure regions to test combustion phenomena, chemistry, and thermodynamics of gas reactions at temperatures up to several thousands of Kelvins in the region near the endwall of the shock tube.

In recent years, relatively long experiments are being employed, such as in Amadio et al. [1], de Vries and Petersen [2], Davidson and Hanson [3], and Hong et al. [4,5]. These experiments are being performed in upwards of 15 ms test times with the continued assumption that the region behind the reflected shock wave can be considered isothermal prior to the main chemical reaction. The isothermal assumption is applicable to short test times as heat transfer between the hot gas and the cold walls does not appreciate significantly, but there is some concern that longer test times, greater than about 5 ms, may potentially allow significant heat transfer to the walls of the shock tube, thus creating observable deviations from the isothermal assumption.

Research performed by de Vries and Petersen [2] using lower-temperature/higher-pressure techniques has shown that ignition delay time measurements can be performed at temperatures as low as 800 K and for relatively long test times. A thorough analysis capturing the significance of heat transfer to the shock-tube wall over long test times is essential to determine the level of test temperature certainty that can be maintained in shock-tube experiments at long test times. The effects of heat transfer on the region behind the reflected shock wave can be analyzed using calculated mean temperature and thermal boundary layer thickness values at intermittent test times to measure thermal boundary layer growth and temperature loss.

Heat loss to the walls of the shock tube has a well-known solution when considering the heat transfer behind the incident shock wave, as in Bromberg [6], Hartunian et al. [7], and Mirels [8,9]. Solution of this incident-shock problem involves convection from the moving gas behind the incident shock wave as transferred to the wall via the moving gas in the growing boundary layer. The focus of these classic problems, however, was on the boundary layer temperature profile and not on the resulting average hot gas temperature.

On the other hand, a closed-form analytical treatment of the wall heat transfer behind the reflected shock wave is difficult. Most of this difficulty is due to the fact that the motion of the reflected shock wave through the gas that has been previously conditioned by the incident wave brings the gas to zero velocity. The induced gas flow that created the growth of the boundary layer behind the incident shock wave is then no longer present, but the fluid in the boundary layer does not necessarily stop moving, as shown by Wilson et al. [10] and Nishida and Lee [11]. The approach taken herein is to first treat the gas/wall interaction behind the reflected shock wave as one of pure conduction, keeping with the assumption that the gas behind the reflected shock wave is stationary. In this way, an analytical model can be developed for parametric studies designed to gauge the effect of test temperature, pressure, tube geometry, and test gas on the heat transfer at long times. The more complex treatment that includes the aftermath of the shock-boundary layer interaction will be treated more thoroughly in a separate paper but is briefly covered in the current paper as well to validate the calculations based on heat conduction alone.

Although the problem of wall heat transfer in shock tubes has been studied often from both an academic and a practical standpoint, no comprehensive evaluations of the effect of heat transfer on the test gas uniformity at long times and in conditions of elevated test pressure were found. In most cases, the emphasis has been on evaluating the increase in wall temperature and the thickness of the thermal boundary layer rather than in the temperature distribution in the core gas region. The present study for the first time evaluates the impact of heat loss to the shock-tube walls in the endwall region using a fully two-dimensional solution in $T(r, x, t)$, with emphasis on the temperature distribution in the entire hot-gas region as a function of test time. Provided in this paper are details on the analytical solution for three different models: (1) the endwall, or $T(x, t)$ solution; (2) the radial heat transfer problem to the sidewall, or $T(r, t)$; and, (3) the heat transfer in the entire endwall region behind the reflected shock wave, or $T(r, x, t)$. Calculations of temperature uniformity in the hot gas region, thermal boundary layer thickness, and wall temperature are provided for the shock-tube geometry of primary interest herein.

2 Heat transfer model

As mentioned above, the primary mode of heat transfer that is assumed to occur in the present study is conduction, which applies to both the hot test gas medium and the cold shock-tube walls. The basic problem is one where the post-shocked, hot test gas is immediately exposed to the cold walls of the shock tube. Hence, at time $t = 0^-$, the gas is assumed to be at temperature T_g, and the walls are assumed to be at the initial temperature T_a. At time $t = 0^+$, the wall and hot gas are in contact and transfer heat via conduction as per Fourier's law of heat conduction

$$\nabla^2 T = \frac{1}{\alpha}\frac{\partial T}{\partial t} \tag{1}$$

Several other assumptions were made when applying the equations in this study. These assumptions include the fact that the test gas is assumed to be an ideal gas; the gas specific heat and thermal conductivity are specified as functions of temperature but are assumed to be constant for a given initial test-gas temperature, T_g, to facilitate solution of Eq. 1;

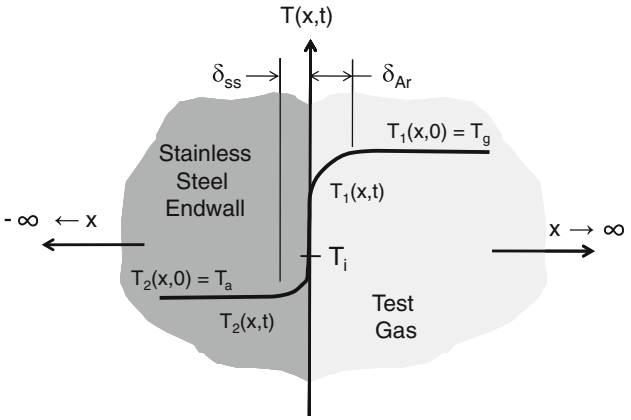

Fig. 1 Endwall region heat conduction model. The hot gas is to the right of the interface, and the cold wall is to the left

chemical reactions are neglected in the gas phase because the focus of the present study is in the gas temperature leading up to the main combustion event; and the motion of the reflected shock wave is neglected, so the initial conditions in the endwall region under consideration are assumed to be after the shock has passed. This latter assumption is valid when one considers the overall time scales of milliseconds after shock passage that are of interest to the present study relative to the time it takes the shock to pass through the gas in the endwall region, which is on the order of hundreds of microseconds. Presented below are brief overviews on each of the closed-form analytical solutions to the endwall region heat conduction problem, that is, the $T(x,t)$, $T(r,t)$, and $T(r,x,t)$ models. Further details are provided in the Appendix.

2.1 $T(x,t)$ solution

For the endwall region of the shock tube, the solution of the $T(x,t)$ problem assumes a semi-infinite solid wall is instantaneously put into contact with a semi-infinite, hot gas. The basic problem is well known for shock tubes, as shown by Goldsworthy [12], Sturtevant and Slachmuylders [13], Baganoff [14], and Hanson [15], among others. Figure 1 presents the basic problem and nomenclature.

As the duration of the test is very brief, there is not enough time for the thermal penetration depth, $\delta_{ss}(t)$, to reach the outside wall of the shock tube. Consequently, the endwall/gas region of the shock tube is modeled herein as two conducting, semi-infinite media each initially at a constant but different temperature suddenly joined at $x = 0$ in perfect thermal contact at $t = 0^+$. The gaseous (right-most) medium 1, for $x > 0$, is taken as the hot test gas with thermal conductivity k_1 and thermal diffusivity α_1, initially at temperature T_g, while medium 2, for $x < 0$, is taken as the solid endwall with thermal conductivity k_2 and thermal diffusivity α_2, initially at temperature T_a, as illustrated in Fig. 1. The solution to this problem and the resulting thermal penetration depth is given by [16,17]. The equations are summarized in the Appendix.

2.2 $T(r,t)$ solution

This problem can be considered as the radial analog of the endwall model, where the region of concern is the shock-tube lateral wall/gas region as illustrated in Fig. 2. The solution for $T(r,t)$ is provided in the Appendix.

Using the resulting $T(r,t)$ radial temperature distribution in the test gas, an average gas temperature can be determined at the desired test time. In this paper, the average test temperature, T_{avg}, is defined as the area-averaged temperature at the axial position of interest (in the radial problem, the average temperature is the same at every axial position). Treating the problem as one of only heat conduction provides a simple estimate of the effects of wall heat transfer at longer test times. To the authors' knowledge, the consideration of the radial heat conduction problem for the conditions behind the reflected shock wave as outlined here has not been previously considered in the shock-tube literature. For relatively large-diameter shock tubes, it is expected that the $T(r,t)$ solution for the thermal layer thickness and temperature distribution should approach that of the 1-D, $T(x,t)$ case considered above; this trend was verified through subsequent calculations.

2.3 $T(r,x,t)$ solution

By combining the radial solution with the endwall solution, the heat transfer in the entire endwall region of the shock tube can be modeled analytically. The time-dependent axial and radial temperature distribution in the test gas (Fig. 3) can be found by use of product solutions as

$$T_1(r,x,t) = T_i + (T_g - T_i)\, S(x,t)\, C(r,t) \tag{2}$$

where

$$S(x,t) = \frac{T_1(x,t) - T_i}{T_g - T_i} \tag{3}$$

$$C(r,t) = \frac{T_1(r,t) - T_i}{T_g - T_i} \tag{4}$$

and $S(x,t)$ is the 1-D semi-infinite medium solution of model 1, while $C(r,t)$ is the 1-D radial solution of model 2 (see Appendix).

3 Model results

Each of the models presented above was applied to a range of temperatures from 800 to 1,800 K for pressures of 1, 20, and 50 atm for a test gas of either pure Argon or pure Nitrogen.

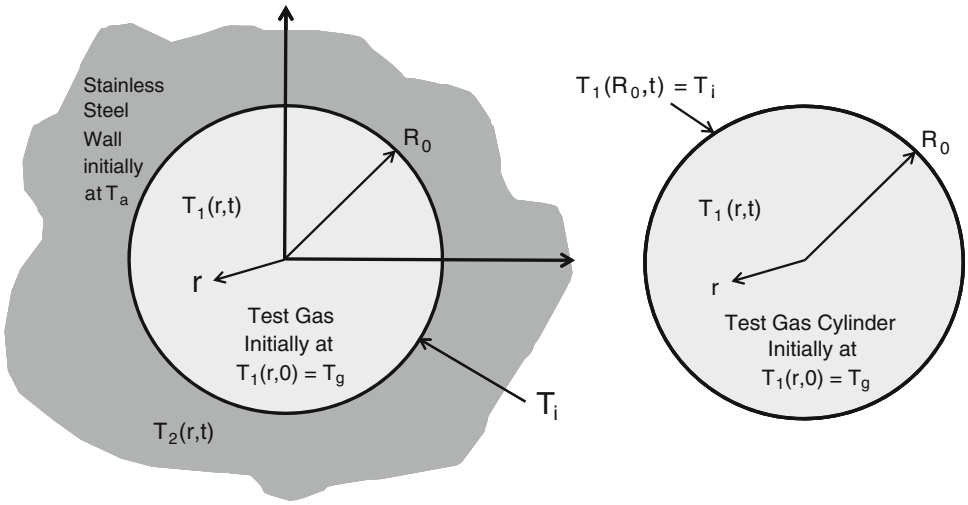

Fig. 2 Radial model of the sidewall/gas interface. Lefthand figure is a gas cylinder in contact with an infinite stainless steel medium. The righthand figure is a gas cylinder imposed with a constant wall temperature, T_i

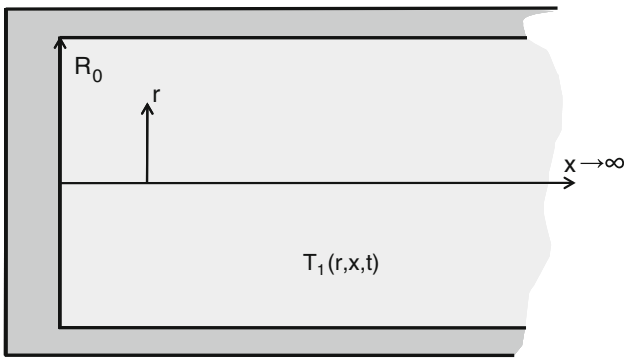

Fig. 3 Distributed model for the gas temperature distribution in the endwall region, $T_1(r, x, t)$

The majority of the calculations presented in this section focused on one specific geometry to coincide with the recent experiments at elevated pressures and intermediate temperatures [1,2] using the facility described by Petersen et al. [18]. In summary, the shock-tube wall material was stainless steel, and the internal diameter of the tube was 16.2 cm with a sidewall thickness of 9.5 mm. Additional calculations were performed in a parametric study to discern the effect of tube inner diameter and location relative to the endwall. These parametric studies on diameter (3, 8.1, and 16.2 cm) and test location (0.5, 1.0, and 1.5 cm) are discussed in more detail later in the paper.

In all calculations, the dependencies of the gas properties on temperature were considered. For the thermal conductivity k, Sutherland's Formula was employed

$$\frac{k}{k_o} = \left(\frac{T}{T_o}\right)^{\frac{3}{2}} \left(\frac{T_o + S}{T + S}\right) \tag{5}$$

where the constants k_o, T_o, and S are were obtained from White [19] and are summarized in Table 1. The constant-pressure specific heat, c_p, was modeled with the standard

Table 1 Constants for use in the Sutherland Formula for thermal conductivity

Gas	T_o (K)	k_o (W/m-K)	S (K)
N_2	273	0.0242	150
Ar	273	0.0163	170

Table 2 Specific heat constants for N_2 and Ar

Const	N_2		Ar
	300–1,000 K	1,000–5,000 K	300–5,000 K
a_1	3.298677	2.926640	2.50
a_2	0.14082404 e-02	0.14879768 e-02	–
a_3	−0.03963222 e-04	−0.05684760 e-05	–
a_4	0.05641515 e-07	0.10097038 e-09	–
a_5	−0.02444854 e-10	−0.06753351 e-13	–

5-parameter polynomial fit

$$\frac{c_p}{R} = a_1 + a_2 T + a_3 T^2 + a_4 T^3 + a_5 T^4 \tag{6}$$

with the constants a_i taken from the Chemkin Thermodynamic Database [20], and R representing the ideal gas constant. Table 2 lists the constants for Argon and N_2. For convenience, Table 3 provides values for c_p, k, and $\alpha = \frac{k}{\rho c_p}$ for both gases at a pressure of 20 atm over a range of temperatures of interest herein.

Figure 4 presents the results of the $T(x, t)$ (endwall) solution. In Fig. 4a, the temperature distribution in the Argon gas near the gas/wall interface is presented for three different pressures (1, 20, 50 atm) at a time of 20 ms after shock passage and for two different initial gas temperatures (800 and 1,400 K). This figure shows the general result that the thermal boundary layer is thinnest at the higher pressures and for the lower initial test gas temperatures. Therefore,

Table 3 Physical properties for Argon and Nitrogen at 20 atm over a range of temperatures

T (K)	Gas	c_p (J/kg-K)	k (W/m-K)	$\alpha \times 10^5$ (m^2/s)
800	Ar	520	0.037	0.590
800	N_2	1118	0.055	0.581
1000	Ar	520	0.043	0.854
1000	N_2	1167	0.064	0.807
1400	Ar	520	0.053	1.476
1400	N_2	1231	0.079	1.321
1800	Ar	520	0.062	2.205
1800	N_2	1271	0.092	1.912

the results of the calculations favor thinner thermal layers (and hence more uniform, high-temperature core regions) at the conditions where longer test times are more likely for kinetics experiments, that is for higher pressures and lower temperatures. Figure 4b plots the thermal layer thickness in the Argon test gas, δ_{Ar}, as a function of time for a pressure of 20 atm and four different gas temperatures. This plot also shows the trend of decreasing thermal layer thickness with decreasing gas temperature, and it also shows that the thickness at the worst-case temperature for this study (1,800 K) is only 2.4 mm at a time of 20 ms.

Additionally, the wall surface temperature experiences a "jump" condition at $t = 0^+$ but this jump is only at most a few degrees for the conditions herein; the wall temperature remains at this value until the thermal layer in the solid reaches the outer wall (which does not happen within the time frame of interest herein). For example, the wall temperature only increases by 3.1 K for the test conditions of 50 atm and 1,400 K. Also of importance is the penetration depth of the thermal layer into the steel wall. For the most extreme condition of 1,800 K and 1 atm, at a time of 20 ms the thermal layer has only penetrated 1.7 mm into the steel wall, per the T(x,t) solution. Hence, the assumption that the thermal layer does not penetrate through the wall in the higher-dimensional models is valid for the conditions of this paper.

For the $T(r, t)$ solution, the thermal layer thickness in the test gas is identical to the solution from the $T(x, t)$ problem because of the relatively large inner diameter of the shock tube modeled (i.e., 16.2 cm). Typical temperature profiles as a function of radius are shown in Fig. 5 for three different pressures (1, 20 and 50 atm) and two different temperatures (800, 1,400 K). The thermal layer thickness can be obtained from the $T(r, t)$ solution and compared to the results from the $T(x, t)$ model. Figure 4b shows the calculations for δ_{Ar} from the $T(r, t)$ model in comparison with the $T(x, t)$ solution at 20 atm. The results are identical for all cases studied, with both solutions overlapping.

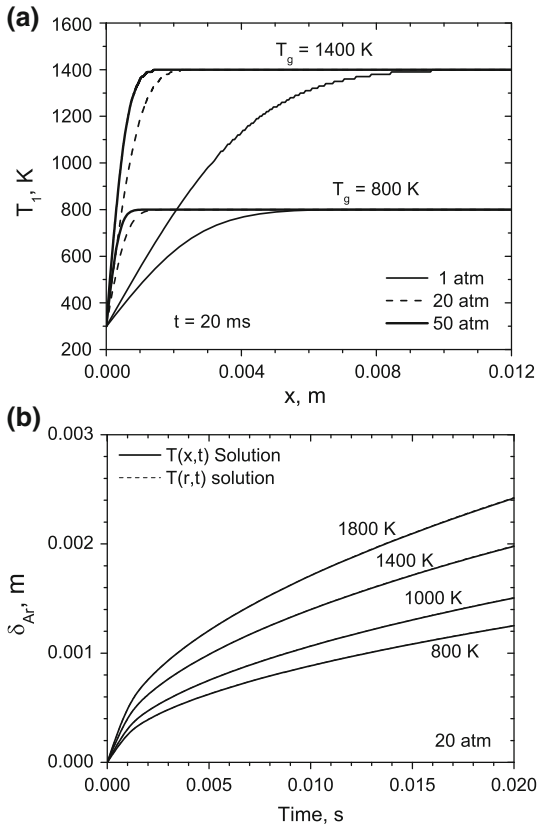

Fig. 4 Calculated results for temperature distribution and thermal layer thickness at 20 ms. **a** $T(x, t)$ solution for Argon gas at two initial temperatures (800 and 1,400 K) and three pressures (1, 20, 50 atm). **b** Thermal layer thickness for $T(x, t)$ and $T(r, t)$ solution at 20 atm. Note that in **b** the $T(x, t)$ and $T(r, t)$ solutions are coincident

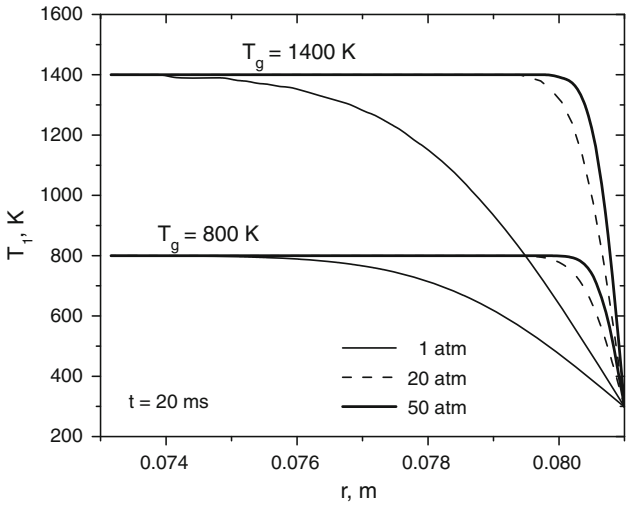

Fig. 5 Calculated temperature distributions for the $T(r, t)$ model for Argon gas at two initial temperatures (800 and 1,400 K) and three pressures (1, 20, 50 atm) at 20-ms test time

More importantly, the radial solution allows for the calculation of an average gas temperature over the entire hot gas region. A typical result is shown in Fig. 6, which displays

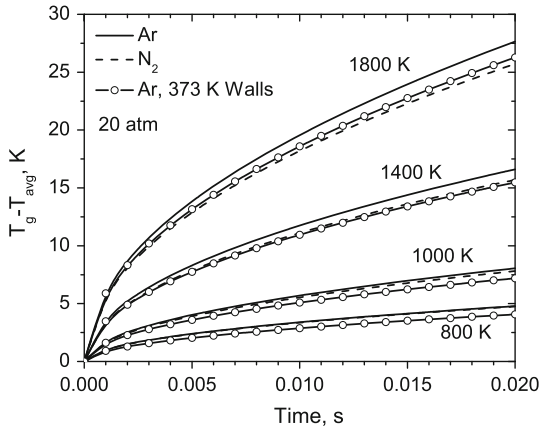

Fig. 6 Decrease in average gas temperature from the radial model for a pressure of 20 atm and four different initial gas temperatures and test gases of Ar and N_2. Tube diameter is 16.2 cm

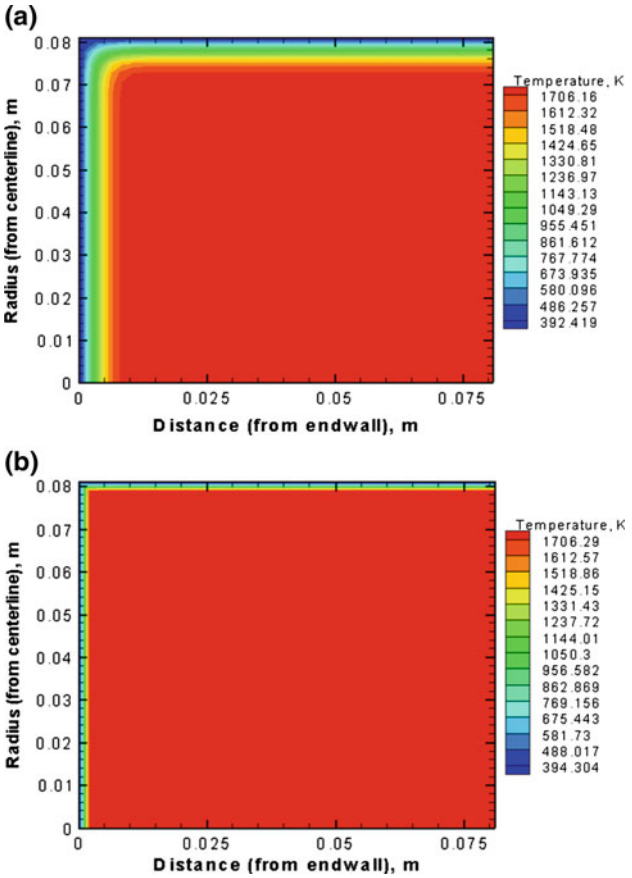

Fig. 7 Complete $T(r, x, t)$ solution for the entire endwall region at $t = 20$ms for an initial test condition of 1,800 K, 1 atm (*upper*, **a**) and 1,800 K, 20 atm (*lower*, **b**). Tube diameter is 16.2 cm, and the test gas is Argon

the change in average gas temperature relative to the initial T_g for a range of temperatures at a pressure of 20 atm. Again, throughout this paper T_{avg} is defined as the area-average temperature at the axial location of interest. Note that at a test condition of 800 K and 20 atm, the average Argon gas temperature only decreases by about 5 K. Also, for a typical shock-tube experiment that ends within 3 ms, the average Argon gas temperature for a 1,400-K experiment at 20 atm decreases by about 6 K.

Studies conducted with N_2 showed that a test region behind the reflected shock wave composed of N_2 would yield a similar although slightly smaller average temperature loss over time than Argon (Fig. 6). Since the gas constant for N_2 is greater than that for Ar, N_2 will always have a lower density ρ (under the same temperature and pressure conditions for each gas) according to the ideal gas equation, $\rho = P/RT$. The effect of the test gas on the heat transfer also shows up in the thermal diffusivity, α. Looking at Table 3 and establishing that the thermal boundary layer grows as a function of thermal diffusivity and time, or $\delta \propto \sqrt{\alpha t}$ [21,22], N_2 has a thinner thermal boundary layer and experiences less average temperature loss due to maintaining a lower thermal diffusivity than Ar for all test temperatures. From Table 3, as temperature increases, so does the value of α, and this trend correlates with the greater thermal boundary layer thicknesses seen at higher test temperatures.

In recent years, these has been interest in experiments with low vapor pressure fuels, requiring a heated shock tube to prevent condensation of the fuel component in the test-gas mixture. It is of interest herein to see how a hotter wall affects the results of the heat loss calculations. Figure 6 shows the results of such a calculation for an initial wall temperature of 373 K for Ar at 20 atm and the four different sample temperatures (800, 1,000, 1,400, and 1,800 K). As shown, the 100-degree hotter walls had minimal impact on the heat loss from the core test gas of the shock tube. Upon closer inspection, the temperature loss for the heated tube is actually a few degrees less than that seen for a room-temperature shock tube because the temperature gradient between the walls and the core gas is smaller.

Finally, the results of both the endwall and sidewall heat transfer are modeled by the $T(r, x, t)$ solution. Two typical results are shown in Fig. 7 for cases with an initial gas temperature of 1,800 K for a test time of 20 ms in Argon. The upper figure is the solution for a lower pressure of 1 atm, and the lower figure is the solution for a higher pressure of 20 atm. The regions of the thermal layers are evident, with the lower-pressure result leading to a thicker thermal boundary layer and, hence, higher temperature non-uniformity than the higher-pressure result. At a suitable distance outside of the endwall thermal layer, the temperature distribution is the same as that predicted by the $T(r, t)$ model for both cases shown in Fig. 7. Of interest to the present study is a location 16 mm from the endwall, where the sidewall optical access port is located for chemical kinetics experiments (more on this aspect below). Figure 7 shows that even in the worst-case

conditions of higher temperature and lower pressure, the hot gas region is effectively outside of the endwall thermal layer even at 20 ms. Further discussion on the test port location is provided below.

One key point that is particulary evident in Fig. 7 is that the core region of the gas remains completely uniform and at the initial gas temperature, T_g. At this point, the reader is also reminded that the results presented thus far are for a specific shock-tube geometry [18] (16.2-cm diameter). Calculations for other geometries (namely, smaller internal diameters) are presented in the following section. Since any convective effects at the sidewall behind the reflected shock wave are neglected in the pure conduction model, we suspect that their inclusion might affect the heat transfer between the hot gas and the solid wall material. Therefore, we conducted a sample calculation including convective effects, the results of which are also presented below.

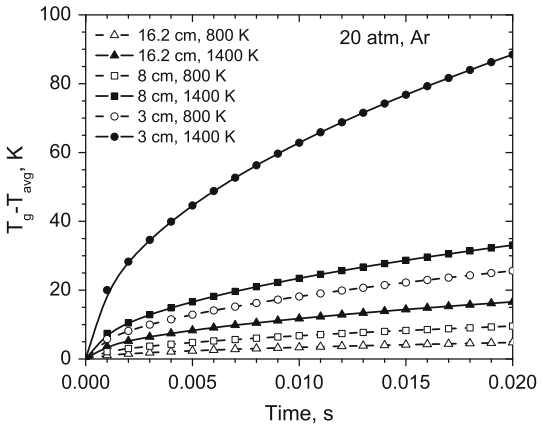

Fig. 8 Average temperature loss over time in Argon, 20 atm, at 800 and 1,400 K for 16.2, 8.1, and 3 cm inner diameters. Average temperature loss increases with smaller diameter, higher temperature, and lower pressure

4 Parametric study

Using the heat conduction model described above, a parametric study was conducted to determine the effect of shock-tube diameter and test port location on the bulk temperature of the gas at long test times. A second study was also conducted to gauge the effect of test port location. Both of these studies are presented in this section, along with a correlation that was developed that combines the results of the present model to predict the average temperature loss as a function of several parameters.

4.1 Shock-tube diameter

As expected upon considering the impact of surface area-to-volume ratio on heat transfer, the size of the inner diameter of the shock tube has a significant effect on the amount of heat transfer losses experienced by the test region. To investigate this phenomenon more fully and to provide results that can be utilized by shock-tube laboratories other than the one of interest herein, a parametric study was conducted for varying tube inner diameters. Since the $T(x, t)$ calculations are for a semi-infinite slab, only the axisymmetric and 2-D solutions depend on the tube diameter. Three diameters were considered in the calculations: 16.2, 8.1 and 3.0 cm. For all three diameters, the wall thickness was maintained at 9.5 mm for simplicity. Since the thermal penetration depth into the walls was never more than a few millimeters, the wall thickness did not affect the parametric calculations.

The results of the parametric study show that reducing the inner diameter of the shock tube from the relatively large one employed herein (16.2 cm) down to 3 cm negatively impacts the temperature profile as predicted from the radial model for all pressures and temperatures. This negative impact is an artifact of the thermal boundary layer thickness relative to the cross-sectional area of the tube. For example, the 20-ms profile at 800 K, 20 atm reaches the initial temperature at approximately 2 mm from the sidewall for all diameters. However, the smaller the inner diameter, the greater the impact on thermal integrity, as the freestream temperature represents a much smaller area of the test region. Figure 8 shows the area-averaged temperature loss over time as the diameter is reduced from 16.2 to 3 cm in Argon at 20 atm for 800 and 1,400 K. A reduction in diameter from 8.1 to 3 cm results in a dramatically higher average temperature loss than a reduction from 16.2 to 8.1 cm.

To summarize, the reason for increased average temperature loss over time as shock-tube diameter decreases is that the thermal boundary layer grows as a function of thermal diffusivity and time and independent of inner diameter. As the thermal boundary layer grows, it occupies a greater amount of the test region area. If the diameter is reduced, the growing thermal boundary layer compromises a larger percentage of the total test region area than if the inner diameter were larger. This trend further suggests that the reduction of shock-tube inner diameter degrades the thermal integrity of the test region behind the reflected shock wave.

Contour plots of the temperature field obtained from the $T(r, x, t)$ solution show best the impact of tube diameter on the relative areas of the thermal layer and the core region of the test gas. Figure 9 shows the temperature distribution in Argon at 1,800 K and 1 atm at a 20-ms test time for all three diameters studied. In each 2-D plot, the temperature field is shown on normalized axial (x/R) and radial (r/R) distance scales. From the three temperature maps in Fig. 9, it is clear that smaller diameters can significantly reduce the thermal integrity of the test region. The same trend was noticed with other temperatures, pressures, and in N_2 as well.

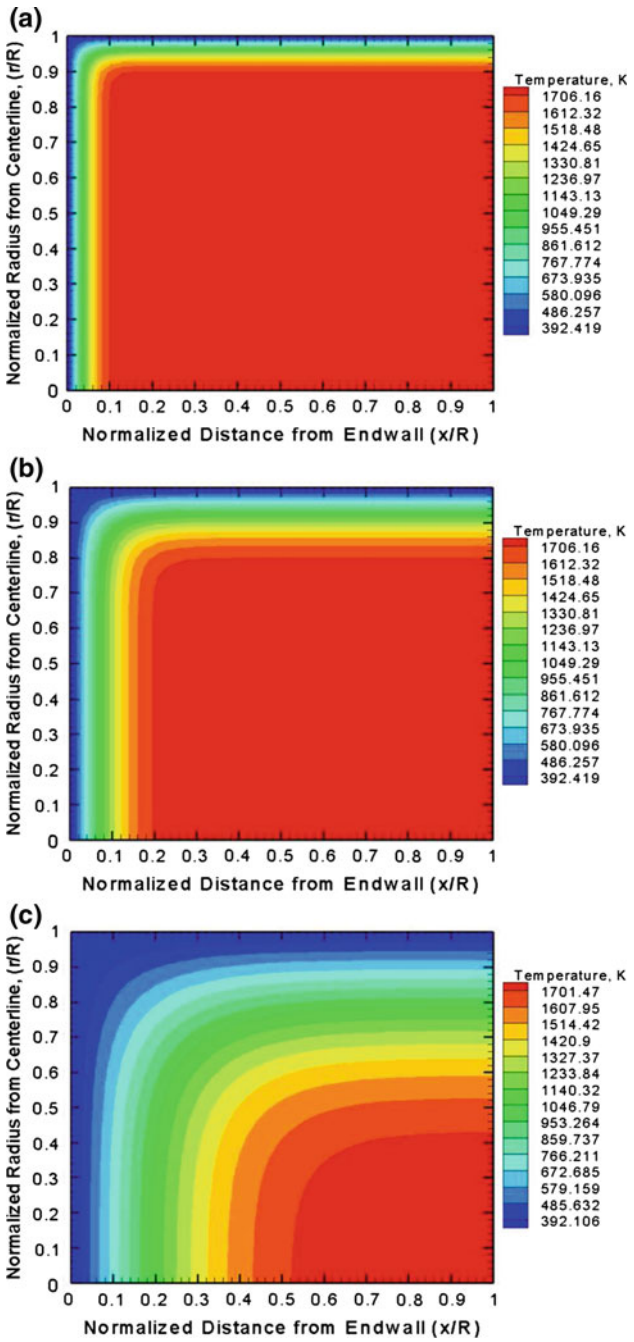

Fig. 9 Contour plots of the temperature distribution within the endwall region behind the reflected shock wave at a 20-ms test time for a tube diameter of **a** 16.2 cm, **b** 8.1 cm and **c** 3 cm. Test gas is Argon, the initial temperature is 1,800 K, and the pressure is 1 atm. The effect of the thermal boundary layer on the thermal integrity of smaller diameters can be seen. The radius and distance from the endwall are normalized to put the temperature distribution on a comparable basis amongst the three diameters

4.2 Test-port location

One common detail in reflected-shock experiments is the location of a sidewall measurement port relative to the endwall. Being as close to the endwall as possible is best for estimating the conditions behind the relfected shock wave, but a port that is too close to the endwall could be within the thermal layer. Hence, the question that is often asked is how far away to place the test port to be within the reliable region for test temperature? To assess the impact of test port location on average temperature maintenance in the test region, average temperatures were calculated using the $T(r, x, t)$ model at specific distances from the endwall, namely 0.5, 1.0 and 1.5 cm. Figure 10 summarizes the results of these calculations.

From Fig. 10a, the calculated results show that using higher pressures renders test port location irrelevant for the three locations studied due to thinner thermal boundary layers at higher pressure. Only at lower pressures, longer test times (>5 ms), and test port locations extremely close (0.5 cm or less) to the endwall does test port location become a factor in receiving accurate data within the test region. For the 1-atm cases, there was no significant average temperature difference (>5%) prior to 5 ms, with the greatest differences being 4 K between the 1.0- and 0.5-cm locations. As test time increases, the differences do grow significantly between the 1.0- and 0.5-cm locations, and the average temperature loss seen at test port locations 0.5 cm or less can be greater than 150 K (Fig. 10b). It should be noted that higher test temperatures experience a significant difference in average test temperature loss at earlier test times (Fig. 10b). The trend was uniform for all cases.

4.3 Temperature-loss correlation

While the heat transfer model described and employed above can be utilized exactly by programming the equations into a suitable algorithm, a more convenient technique for readers interested in estimating the average temperature loss in their shock tube would be if the results in this paper could be combined into a single, empirical correlation. Just such a correlation that describes the $T(r, t)$ model results surprisingly well was found, discussed as follows.

To estimate the average temperature loss in the test region as a function of time and the parameters of interest herein, i.e., test temperature, test pressure, shock-tube inner diameter, and gas characteristics, a correlation was developed for $\Delta T_{\text{loss,avg}} = f(t, D, T_g, \rho, k, c_p)$. Based on the parametric study results described above, it was noticed that the average temperature loss grew in proportion to $\sqrt{\alpha t}$, much like the same relationship exhibited for the thermal boundary layer thickness from previous research [21,22]. A suitable correlation that best fit the results over the entire range of conditions utilized in this study (i.e., $800 < T_g < 1{,}800$K, $1 < P < 50$ atm, Ar, N_2, $0.001 < t < 0.020$ s,

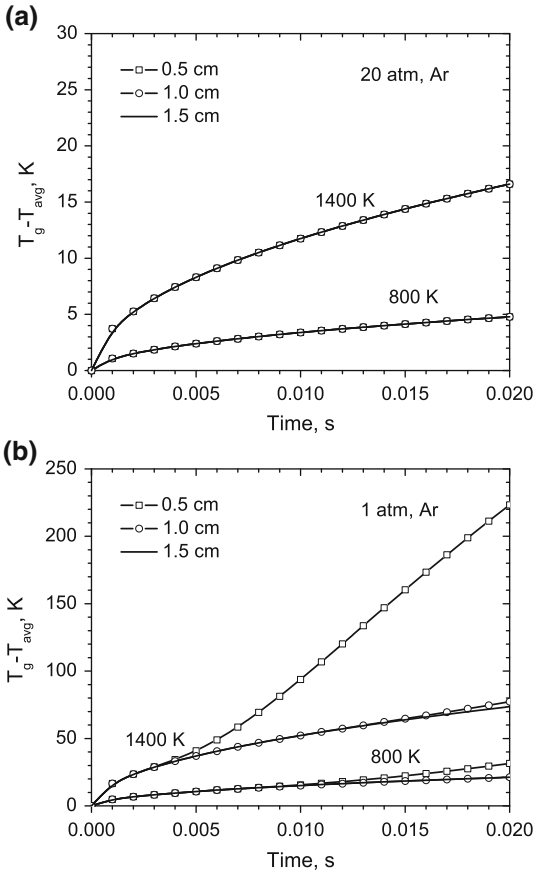

Fig. 10 Average temperature loss over time within the test region in Argon, at 800 and 1,400 K for three test port locations from the endwall (0.5, 1.0, 1.5 cm). Figure **a** is for 20 atm and **b** is for 1 atm. Note that in **a** the results for each port location are identical; similar overlap occurs in **b**, except for the 1,400 K case above 0.005 seconds

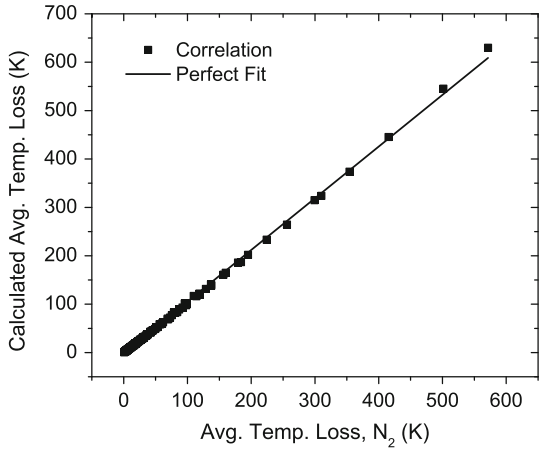

Fig. 11 Comparison of the correlation in Eq. 7 with the calculated results of average temperature loss from the full $T(r, t)$ model. Test gas is Nitrogen, and the range of conditions are $800 < T_g < 1{,}800$ K, $1 < P < 50$ atm, Ar, N_2, $0.001 < t < 0.020$ s; and $0.03 < D < 0.162$ m

and $0.03 < D < 0.162$ m) was found to be:

$$\Delta T_{\text{loss,avg}} = T_g - T_{\text{avg}} = \frac{0.29685 T_g{}^{1.34}}{D}\sqrt{\alpha t} \tag{7}$$

where T_g is in K, D is in m, α is in m^2/s, and t is in seconds. Equation 7 describes the $T(r, t)$ results remarkably well and is relatively easy to apply. Figure 11 shows how well the correlation fits the calculated $\Delta T_{\text{loss,avg}}$ results for a Nitrogen test gas. Each point in Fig. 11 represents a result from the full $T(r, t)$ model at discrete levels of T_g, P, and D over the range of interest in this paper. The statistical goodness of fit parameter, or r^2, for the predictions of the correlation is 0.99.

4.4 Two-zone model

As mentioned above, the results of the radial heat conduction model indicate that the core temperature of the gas remains at the initial post-shock temperature, T_g. This result, however, is based on the heat conduction solution that treats both the gas and the wall as solid bodies. In the real situation, the gas will migrate from the hot core to the cold thermal boundary layer as the layer grows in thickness. Also, the reader should not confuse the average loss in temperature used herein ($\Delta T_{\text{loss,avg}}$) with the main core gas temperature, T_{core}. Recall that the average temperature as defined above is the area-averaged temperature that includes both the core gas T_{core} (or T_g for the two-body conduction solution above) and the cooler gas through the thermal layer of thickness δ. Also of interest for chemical kinetics experiments is the test-gas pressure. In the heat conduction model outlined in the previous sections, the pressure only entered the calculation through the thermal diffusivity, which was assumed to be constant and equal to the α at the initial, post-shocked conditions. However, in the real gas, the pressure will decrease with time as the thermal boundary grows due to the loss of density from the core region to the growing thermal layer.

This change in pressure can be modeled by dividing the problem into two main regions, as shown in Fig. 12. The simple model has the core region at temperature T_{core} with the thermal layer near the walls of thickness δ at an average temperature T_δ. The thickness of the thermal layer, defined at the radial position where the temperature is within 99% of the core temperature, can be obtained from the solution to the $T(r, t)$ model. Over the range of conditions used in the parametric study above, a correlation for δ was found to be simply

$$\delta = 3.6113\sqrt{\alpha t} \tag{8}$$

Hence, the thermal layer, as expected, grows in proportion to the square root of the thermal diffusivity times the time. The two-zone model shown in Fig. 12 is maintained until the thermal layers ultimately merge and eliminate the uniform-temperature core region. Of course, the full solution to $T(r, t)$ is known from the heat conduction and can be used in lieu

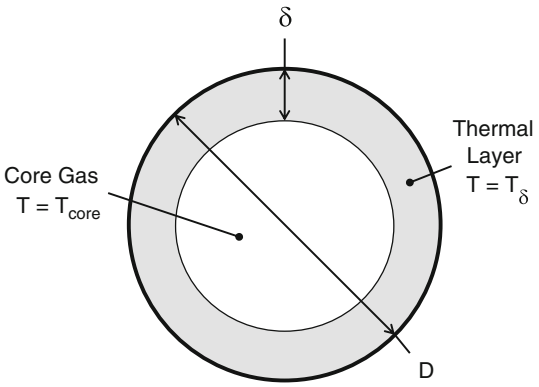

Fig. 12 Diagram of two-zone radial model, showing the core at temperature T_{core} and the thermal layer of thickness δ at an average temperature of T_δ

of the simple 2-zone model, but this solution assumes the core temperature remains at T_g and the gas pressure remains at P_g.

To obtain the pressure as a function of time, one must consider the following constraints: (1) the pressure is the same throughout the radial cross section, that is, $P_{\text{core}} = P_\delta = P$; (2) the temperature profile through the thermal layer is known from the heat transfer solution; and, (3) the overall density ρ (or mass m per volume V of gas) for the problem is constant and equal to the initial condition

$$\rho = \frac{m}{V} = \frac{P_g}{RT_g} = \text{constant} \tag{9}$$

where R is the ideal gas constant. The sum of the mass of gas in each zone must at all times be equal to the total mass, or

$$\frac{P_g V}{RT_g} = \frac{P V_{\text{core}}}{RT_{\text{core}}} + \frac{P V_\delta}{RT_\delta} \tag{10}$$

For the radial solution with $V = \pi D^2 L/4$, Eq. 10 can be solved for the pressure change relative to the initial pressure

$$\frac{P}{P_g} = \frac{D^2}{T_g}\left[\frac{(D-2\delta)^2}{T_{\text{core}}} + \frac{D^2-(D-2\delta)^2}{T_\delta}\right]^{-1} \tag{11}$$

For the average temperature in the thermal layer, T_δ, we can use the temperature distribution from the full solution and area average it. However, we have this information built into the temperature loss correlation of Eq. 7, where $T_{\text{avg}} = T_g - \Delta T$. In the two-zone model that treats the core as a gas, the average gas temperature can be put in terms of T_{core} rather than T_g. The average temperature calculation can be divided into the two zones of the present model,

$$T_{\text{avg}} = \frac{\int T\,\mathrm{d}A}{\int \mathrm{d}A} = \frac{2}{R^2}\int_0^{R-\delta} T_{\text{core}} r\,\mathrm{d}r + \frac{2}{R^2}\int_{R-\delta}^{R} T r\,\mathrm{d}r \tag{12}$$

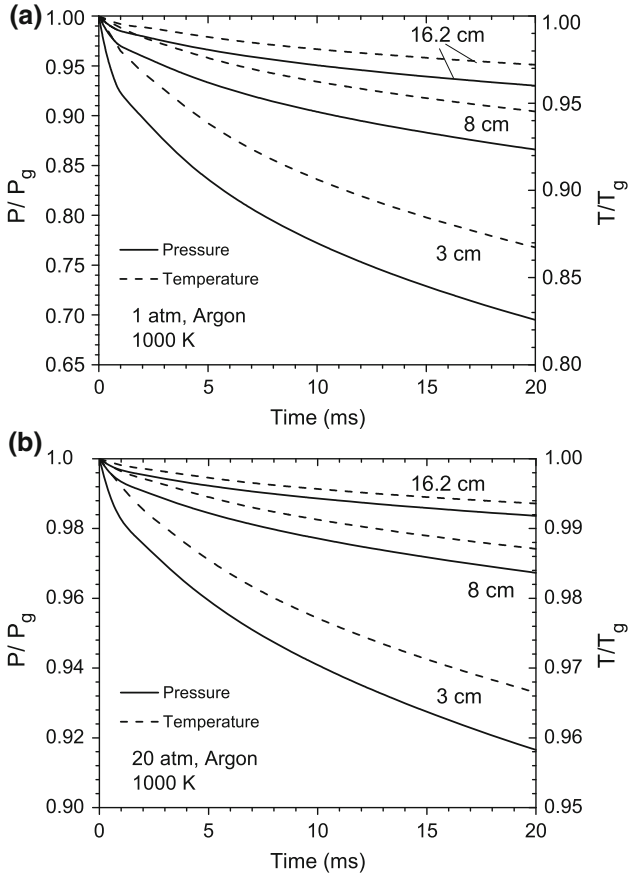

Fig. 13 Change in pressure and core gas temperature over time using the two-zone model. Conditions are for various shock-tube diameters with an Argon test gas at an initial temperature of 1,000 K and pressure of **a** 1 atm and **b** 20 atm

where in the above equation, R is the overall radius of the shock tube, or $D/2$. For an average T_δ over the wall zone, Eq. 12 can be integrated and solved for T_δ as follows

$$T_\delta = \frac{D^2 T_{\text{avg}} - T_{\text{core}}(D-2\delta)^2}{D^2-(D-2\delta)^2} \tag{13}$$

When the average temperature through the thermal layer is determined from the results of the full solution, it agrees with the calculation obtained from Eq. 13 to within about 1 K. The final assumption that needs to be made is how the core gas temperature changes when the pressure changes. In the present method, it will be assumed that the core behaves adiabatically, so that the temperature change is related to the pressure change via the isentropic relation using the specific heat ratio γ as follows

$$T_{\text{core}} = T_g\left(\frac{P}{P_g}\right)^{\frac{\gamma-1}{\gamma}} \tag{14}$$

Using Eqs. 7, 8, 11, 13, and 14, the pressure can be calculated as a function of time. Figure 13 shows some sample calculations for a shock tube with Argon as the test gas at an

initial temperature of 1,000 K for pressures of 1 and 20 atm for three different tube diameters. The test pressure and core gas temperature both decrease with time, with the extent of the decrease being worse for the smaller tube diameters. Note in Fig. 13b that the decrease in pressure and temperature at the higher initial pressure of 20 atm is much less than at the lower-pressure case in Fig. 13a.

5 Effect of boundary layer convection

One major assumption that was made in applying the heat conduction models described above is that the test gas behind the reflected shock wave interacts with the shock-tube walls via conduction heat transfer only. This approach allows for a system of equations that have a closed-form solution so that parametric studies and quick calculations can be performed to assess the effect of heat loss to the walls on reflected-shock test conditions at long test times. However, to gauge the effect that a viscous, moving boundary layer behind the reflected shock wave has on the temperature uniformity of the test gas, a limited set of computational fluid dynamic (CFD) calculations was performed, as discussed in this section. More details on the authors' CFD modeling of shock-tube flow fields can be found in Lamnaouer et al. [23].

5.1 CFD model

To correctly predict the thermal field in the test region of the shock tube, the conjugate heat transfer (CHT) approach was adopted. The heat transfer was computed by coupling the conduction of heat through the shock-tube solid wall thickness with convective heat transfer in the fluid. Therefore, two zones were specified in the grid generation, the solid and the fluid zones. Here the wall thickness must be meshed, and the coupled thermal boundary condition is available on the wall zone which separates two cell zones. As such, the wall thermal resistance is directly accounted for in the energy equation. The boundary between the two zones is always a wall, and a shadow zone is created automatically by *FLUENT*.

The numerical simulations of the fluid flow and heat transfer in the shock tube were accomplished by solving the conservation equations of mass, momentum, energy, and species. Of interest to the current study is the energy transport equation for non-reacting flows which is given by

$$\frac{\partial(\rho E)}{\partial t} + \nabla \cdot \left[\overrightarrow{V}(\rho E + P)\right] = \nabla \cdot \left[k_{\text{eff}} \nabla T - \sum_j h_j J_j + (\tau_{\text{eff}} \overrightarrow{V})\right] \quad (15)$$

where $E = h - P/\rho + V^2/2$ is defined as the energy per unit mass in terms of pressure work and kinetic energy, h is the sensible enthalpy, and V is the absolute velocity. The three terms on the right hand side of Eq. 15 represent energy transfer due to conduction, species diffusion, and viscous dissipation, respectively. The heat flux due to conduction is given by $\nabla \cdot k_{\text{eff}} \nabla T$, where k_{eff} is the effective conductivity and is equal to $k + k_t$; k_t is the turbulent thermal conductivity. The species diffusion term is given by $\nabla \cdot \sum_j h_j J_j$ and includes the effect of enthalpy transport due to species diffusion. J_j is the diffusion flux of species j. The viscous dissipation term is given by $\nabla \cdot (\tau_{\text{eff}} \overrightarrow{V})$. Also called the viscous heating, this term describes the thermal energy created by viscous shear (τ_{eff}) in the flow. An energy source is only included when reactive flow is modeled. In this model, only non-reactive flow is considered.

In the solid region, the conduction of heat is modeled by the following energy equation:

$$\frac{\partial(\rho h)}{\partial t} = \nabla \cdot (k \nabla T) \quad (16)$$

The full shock tube was simulated with the commercial CFD code *FLUENT 6.3*. The geometry of the shock tube and boundary conditions used in this calculation are shown in Fig. 14. Note that the shock tube modeled with the CFD solution is very similar to the baseline shock tube considered above and is based on the facility described in detail by de Vries et al. [24]. One exception is that the driver section is extended from its original length of 2.46 to 4 m to more easily obtain the longer test times of interest in this paper. The driven tube is 4.72 m long. The internal diameters are 7.62 and 15.24 cm for the driver and the driven sections, respectively. The shock tube side wall has a thickness of 1.27 cm, and the endwall is 2.54 cm thick.

Meshing of the geometry was performed in *GAMBIT*, and a structured grid was used to mesh the model for the CFD simulations. The whole computational domain was meshed using approximately 130,000 cells. This mesh resolution was determined after the solution was checked for grid independency. Additional cells were added in the flow domain as necessary via grid adaption to maintain finer mesh around the shock and contact discontinuities. As such, the computational efforts were focused around high-gradient flow fields by keeping the overall computational time to a minimum. The total mesh size increased to approximately 300,000 nodes with grid adaption. Cell distribution was chosen carefully to take into account the effect of the thermal boundary layer on the heat transfer results. Because of the axial symmetry of the shock tube, the geometry was modeled as axisymmetric. This condition imposes a zero normal velocity and zero tangential force along this boundary. An interface condition was set at the diaphragm location at the time of diaphragm rupture. This condition ensured continuity of all physical properties along the interface.

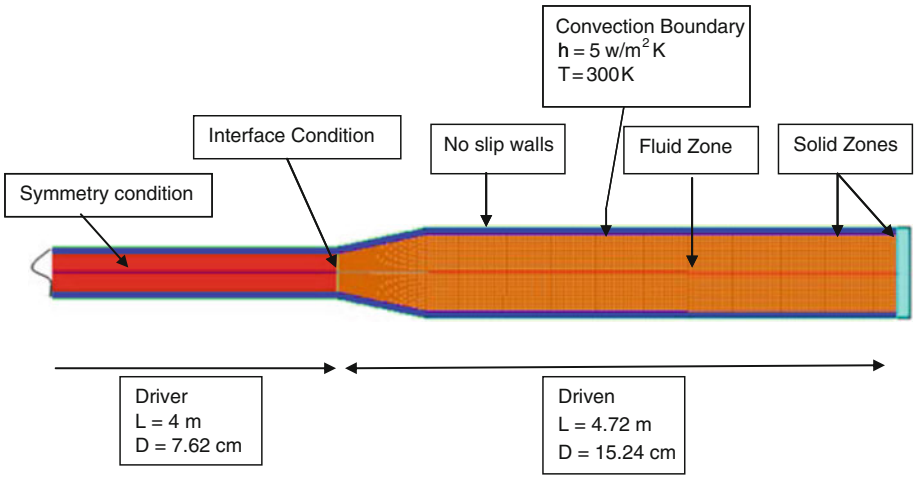

Fig. 14 Shock-tube axi-symmetric mesh and boundary conditions for the full CFD solution calculation

For the CHT simulation, the primary goal was to set the shock-tube driver and driven initial conditions such that they would produce a long test time behind the reflected shock wave at the conditions herein that produced the most extreme change in average test temperature at long times for an 800-K test, which occurs at a 1-atm pressure condition in Argon. Initial conditions were set to a pressure of 3.19 atm and temperature of 300 K in the driver. As for the driven section, a pressure of 0.11 atm and temperature of 300 K were imposed. A convection boundary was applied to the outside shock-tube wall with a heat transfer coefficient of $5\mathrm{W/m^2K}$ and a freestream temperature of 300 K (Fig. 14). The shock-tube wall material is stainless steel with a density of $8{,}030\mathrm{kg/m^3}$, constant specific heat of 502.48 J/kg-K, and thermal conductivity of 16.27 W/m-K. The shock-tube wall temperature was initially set to 300 K. Thermophysical setup of the compressible flow assumes ideal gas density and uses the mixing law for constant specific heat. The thermal conductivity was set to 0.0454 W/m-K, the viscosity to $1.72 \times 10^{-5}\mathrm{kg/m\text{-}s}$, and the mass diffusivity to $2.88 \times 10^{-5}\ \mathrm{m^2/s}$. As viscous effects were incorporated into the CFD model, the boundary layer behind the incident shock wave was modeled, thus allowing for pressure/density changes in the core fluid due to mass loss to the boundary layer.

The coupled problem of unsteady compressible flow and heat conduction in the shock-tube wall material was modeled by the means of the density-based explicit solver with explicit time stepping. The viscous solution was obtained for both the laminar and the turbulent models with the same initial conditions. The *AUSM+* flux vector splitting scheme was used. Discretization in space was based on the 1st–2nd order blending scheme for the laminar model and on the high-resolution, 2nd-order *TVD* scheme for the turbulent model. A purely 2nd-order solution for the laminar model was difficult to achieve and produces nonphysical behavior associated with reconstructing higher-order gradients across the shocks which leads to overshoots and undershoots in the solution. The solution was marched in time by a four-stage Runge-Kutta scheme for unsteady flows, and the time step size was limited by the Courant–Friedrich–Lewy stability condition, which ranged between 0.8 and 1. Further details on the laminar and turbulent models can be found in Lamnaouer et al. [23].

5.2 CFD results

Several runs were performed with different driver-gas mixture compositions to achieve the longest test time possible at the conditions of 800 K and 1 atm. Test times can be extended up to 20 ms by the use of unconventional driver gases such as C_3H_8/He, CO_2/He, or a combination of C_3H_8/CO_2/He mixtures as have been shown by Amadio et al. [1]. A driver mixture composition of 40% C_3H_8 + 60% He provided the longest test time of 15 ms. Figure 15 displays the full turbulent conjugate solution of the shock-tube flow field at 4 snapshots in time (−3, 3, 6, 15 ms after shock reflection) for the temperature, pressure, and Mach number results. By modeling the entire shock tube, the flow details such as the interaction of the reflected shock wave with the contact surface are fully resolved. Of most importance for the problem at hand are the test gas conditions near the endwall region.

Temperature contours are presented in Fig. 16 for the entire test region behind the reflected shock wave for the turbulent solution, corresponding to the 15-ms solutions for temperature, pressure, and Mach number presented in Fig. 15. The heat transfer from the hot gas to the walls is depicted by the thermal boundary layer present along the test region shock-tube walls (Fig. 16a) and appears similar to the predictions of the analytical heat conduction $T(x, r, t)$ model seen in Fig. 7. The temperature distribution shows that the thermal boundary layer is well outside of the test region indicating that heat transfer is not a concern for reflected-shock

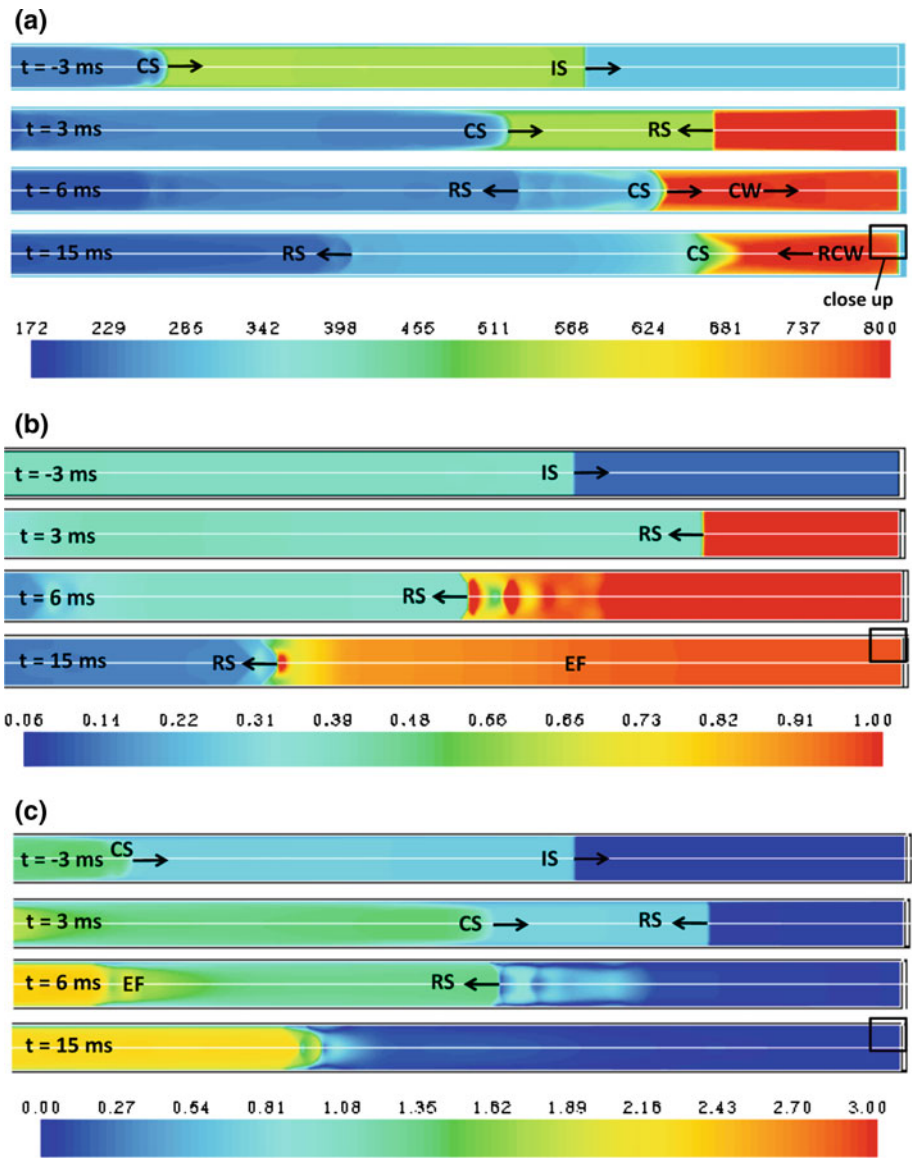

Fig. 15 Turbulent conjugate heat transfer solution showing **a** temperature, **b** pressure and **c** Mach number flow fields during shock propagation, reflection, interaction with the contact surface, and arrival of the expansion fan. Conditions behind the reflected shock are 800 K, 1 atm in Ar test gas. Corresponding times are given in the *upper left corner* of each frame. Time zero is the moment the incident shock reflects off the endwall. *IS* incident shock, *CS* contact surface, *RS* reflected shock, *CW* compression wave, *RCW* reflected compression wave, *EF* expansion fan

experiments at long test times, at least up to 20 ms. This general result of the full CFD simulation confirms the results inferred from the conduction analysis presented above for the baseline shock-tube geometry with a 16.2 cm driven tube diameter. The endwall-region contours of pressure and Mach number in Fig. 16b, c shows that the test gas has a nearly uniform pressure with essentially no bulk movement, even at the extreme test time of 15 ms.

Figure 17 shows the endwall static pressure versus time for the reflected-shock conditions of 800 K and 1 atm. The test time is ended by the arrival of the contact surface expansion wave to the endwall followed by the head expansion wave denoted by the discontinuity in the slope of the pressure trace. The small compression bump near a test time of 5.2 ms is from the interaction of the reflected shock wave with the contact surface, which emits a weak compression wave that travels back toward the endwall, as shown in more detail in Fig. 15.

Heat transfer results are post-processed behind the reflected shock wave over the entire endwall test region. Figure 18 shows the variation in the gas average temperature in relation to the initial gas temperature at the conditions of 800 K and 1 atm in comparison to the analytical $T(r, t)$ conduction model. The conduction solution predicts a larger decrease in the average temperature, indicating a higher loss in temperature than the CHT model. Both models predict a jump in temperature immediately after the solid wall comes into contact with the hot gas, with the jump being more distinct in the CHT viscous results. The higher initial temperature jump at $t = 0^+$ is due to the additional heat transfer between the hot gas and cold wall via the moving boundary layer that was formed initially

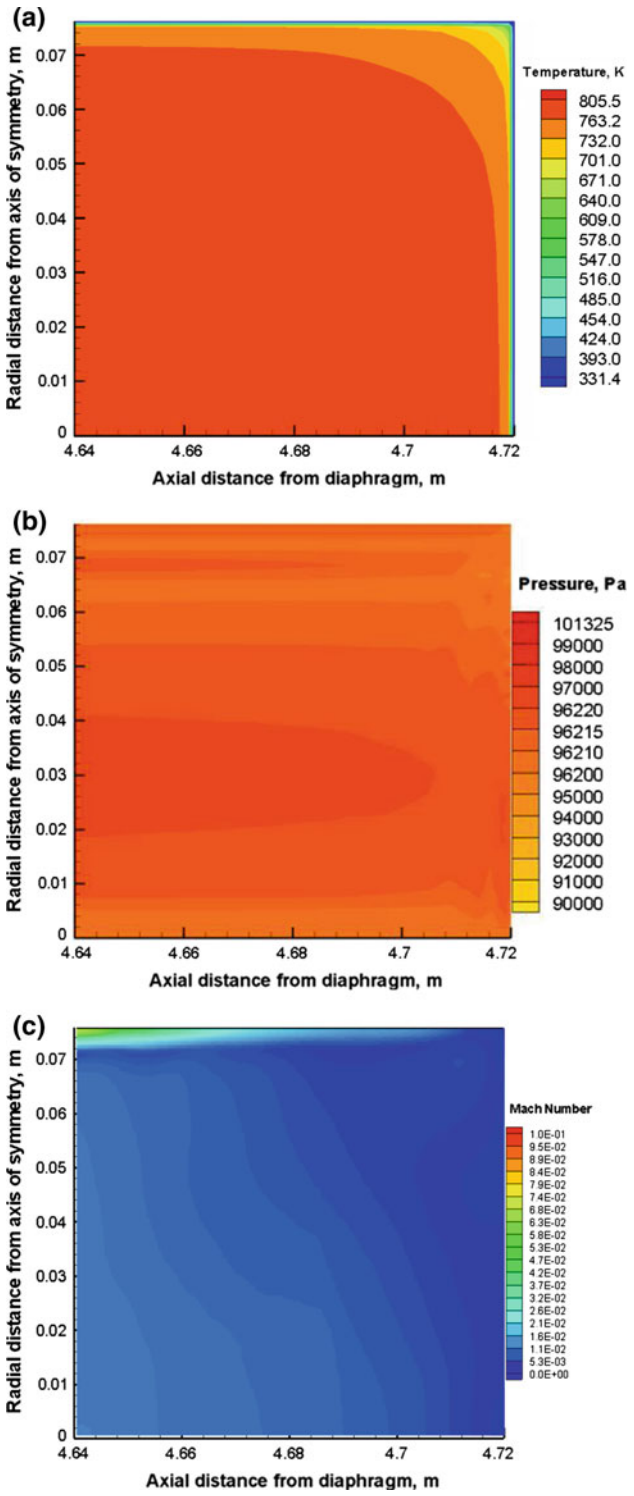

Fig. 16 A close-up on the turbulent conjugate heat transfer solution of **a** temperature, **b** pressure and **c** Mach number flow fields in the Ar hot gas test region at the conditions of 800 K, 1 atm and 15 ms of test time. Each contour corresponds to the *upper right corner* of the flow fields depicted in Fig. 15

behind the incident shock wave. This convective motion of the hot gas is of course not modeled in the conduction-only solution.

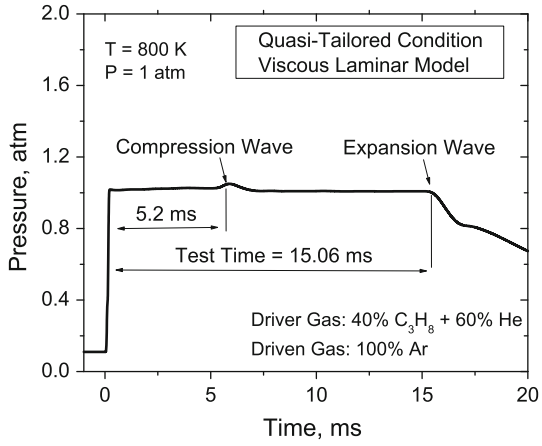

Fig. 17 Endwall pressure time history for the non-reacting, viscous CFD model. Conditions behind the reflected shock are 800 K and 1 atm with 40% propane and 60% He as the driver gas and 100% Ar as the test gas. A test time of 15 ms is achieved

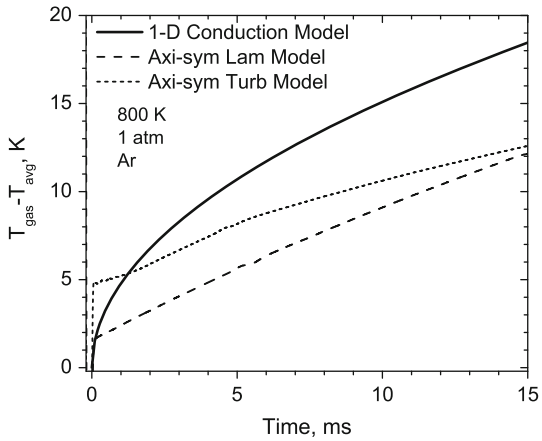

Fig. 18 The difference between the maximum and the average gas temperatures as predicted by the viscous CFD model and comparison with the analytical conduction model. The endwall test region conditions are 800 K and 1 atm in Argon. The maximum gas temperature decreases by 13 K after 15 ms of test time for both the laminar and viscous solutions, versus 19 K for the conduction model

Note also that the turbulent solution predicts a higher initial jump in temperature (by about 3 K) than the laminar solution, a result that also agrees with the reasoning above because of the stronger convective forces in the turbulent boundary layer compared to the laminar one. The conduction model on the other hand exhibits more decrease in the average gas temperature and therefore more heat loss to the shock tube walls. At 15 ms, the average gas temperature decreases by 19 K for the conduction model versus only 13 K for both the laminar and turbulent CFD solutions. The difference in the results can be explained by the presence of the viscous dissipation term in the energy equation, which reduces the net effect of heat transfer at times after initial passage of the reflected shock wave, resulting in less heat loss predicted by

the CHT viscous model. Note that the change in temperature plotted in Fig. 18 is for the average gas temperature; using the two-zone heat conduction model described in the previous section, the corresponding decrease in the core temperature after 15 ms is just under 15 K, which is about 4 K less than the 19-K loss in average temperature predicted by the conduction model.

In summary, the full CFD solution of the heat transfer behind the reflected shock wave at long test times provides a good check on the results predicted by the analytical heat conduction model. Both models predict an average loss in temperature within a few K of each other, with the conduction solution being on the conservative side of over estimating the heat loss. While the full CFD solution provides a more accurate representation of the moving boundary layer and its effects on the wall heat transfer, the solution of even a single case still takes a considerable length of physical time when compared to the solution of the heat conduction model. Hence, the parametric study of the effect of test conditions, test gas, and shock-tube geometry on the heat loss at long test times was more easily performed with the simpler solution with little loss in accuracy, giving very useful results. Even more useful and easier to implement for quick calculations is the temperature-loss correlation provided as Eq. 7.

6 Summary

A heat conduction model was developed for estimating the test gas temperature behind the reflected shock wave in a shock tube during relatively long experiments lasting 15 ms or more. Three conduction models were presented, one for the $T(x,t)$ problem, the $T(r,t)$ problem, and the 2-D $T(r,x,t)$ problem. Calculations were performed for the baseline tube geometry $D = 16.2$ cm over a range of test conditions from 800 to 1,800 K and 1 to 50 atm for a test gas of either Ar or N_2. The thermal boundary layer thicknesses at the wall as obtained from each model were identical amongst the three solutions. Of most interest were the results that characterized the average temperature loss of the test gas, and the radial $T(r,t)$ model provided estimates that indicate that the average temperature (taken over the entire radial cross section) changes by about 25 K at 1,800 K, 1 atm over a period of time of 20 ms. At more realistic conditions for a long test-time experiment (800 K and 20 atm), the average temperature loss is expected to be much less, about 5 K. The results of the $T(r,x,t)$ model near the endwall showed that a test port located at least 1.0 cm away from the endwall would be free of the thermal layer for the baseline shock tube over the entire range of conditions explored herein. Although the average temperature over the entire diameter decreases due to the thermal boundary layer, the main core temperature does not change at all and remains at the initial, post-shock state due to the assumption in the conduction model that both the gas and wall behave as solid bodies. A simple two-zone model that accounts for density loss from the core region to the colder layer near the wall indicates that both the pressure and core gas temperature actually decrease slightly with time, the extent of which depends adversely on the tube diameter.

The closed-form solutions of the conduction heat transfer model allowed for the convenient comparison of shock-tube geometries ($D = 3$–16.2 cm) in addition to the effect of test temperature and pressure. It was found that the smaller-diameter cases resulted in potentially significant temperature losses (80 K or more at 20 atm) at times approaching 20 ms. One key result of the present study was the development of a simple correlation that describes the average test-temperature in a shock tube as a function of α, t, D, and T. This correlation can be easily used to estimate the heat loss for shock tubes operating within the limits of the work herein.

Finally, a sample calculation using a CFD solution of the flow field of an entire shock tube was used to validate the results of the heat conduction model. The full time-dependent CHT solution for a reflected-shock test at 800 K, 1 atm in Argon compared well with the analytical heat conduction solution for the same conditions. Both the laminar and turbulent CFD solutions produced average temperature losses that were about 5 K less than that predicted by the conduction model, implying that the simpler conduction model provides a somewhat conservative estimate of the heat loss.

Acknowledgments This work (TAMU) was funded in part by the National Science Foundation, grant number CBET-0832561.

Appendix

$T(x,t)$ solution equations

Enforcing continuity of temperature and heat flux at the interface,

$$T_1(0,t) = T_2(0,t)$$
$$-k_1 \left.\frac{\partial T_1}{\partial x}\right|_{(0,t)} = -k_2 \left.\frac{\partial T_2}{\partial x}\right|_{(0,t)} \tag{17}$$

the temperatures in each medium are, respectively [16,17]

$$for\ x > 0: \quad T_1(x,t) = T_a + \frac{T_o}{1 + \frac{k_2\sqrt{\alpha_1}}{k_1\sqrt{\alpha_2}}}\left[1 + \frac{k_2\sqrt{\alpha_1}}{k_1\sqrt{\alpha_2}}\mathrm{erf}\left(\frac{x}{2\sqrt{\alpha_1 t}}\right)\right]$$
$$for\ x < 0: T_2(x,t) = T_a + \frac{T_o}{1 + \frac{k_2\sqrt{\alpha_1}}{k_1\sqrt{\alpha_2}}}\left[1 - \mathrm{erf}\left(\frac{|x|}{2\sqrt{\alpha_2 t}}\right)\right] \tag{18}$$

where $T_o = T_g - T_a$ and erf(x) is the error function. Evaluating the interface temperature, T_i, at $x = 0$, reveals that it remains constant until the thermal penetration depth reaches the left, outside wall of the solid endwall and it is given by [16,17],

$$T_i = T_a + T_o\left(\frac{k_1\sqrt{\alpha_2}}{k_1\sqrt{\alpha_2} + k_2\sqrt{\alpha_1}}\right) \tag{19}$$

Results from computations under the test conditions reveal that the thermal penetration depth in the endwall material, $\delta_{ss}(t)$, is much smaller than the endwall thickness at all times under consideration.

6.1 $T(r, t)$ solution equations

The radial temperature distributions corresponding to the model in Fig. 2 can be obtained by means of Laplace transforms, and they are given as complicated functions of integrals on $[0, \infty]$ of Bessel functions of the first kind, J_ν, and second kind, Y_ν, of order ν as well as the conductivity and thermal diffusivity ratios [17] as

$$\begin{aligned}
T_1(r,t) &= T_g \\
&+ (T_g - T_a)\frac{4\rho_k}{\pi^2}\int_0^\infty \frac{J_1(\mu)J_o(\frac{\mu r}{R_o})}{\mu^2[\phi(\mu)^2 + \psi(\mu)^2]} e^{-\mu^2 Fo} d\mu \\
T_2(r,t) &= T_g + (T_g - T_a)\frac{2\rho_k}{\pi} \\
&\times \int_0^\infty \frac{J_1(\mu)\left[J_o\left(\sqrt{\rho_\alpha}\frac{\mu r}{R_o}\right)\phi(\mu) - Y_o\left(\sqrt{\rho_\alpha}\frac{\mu r}{R_o}\right)\psi(\mu)\right]}{\mu[\phi(\mu)^2 + \psi(\mu)^2]} \\
&\times e^{-\mu^2 Fo} d\mu
\end{aligned} \tag{20}$$

where

$$\begin{aligned}
\rho_k &= \frac{k_1}{k_2} \qquad \rho_\alpha = \frac{\alpha_1}{\alpha_2} \qquad \mathrm{Fo} = \frac{\alpha_1 t}{R_o^2} \\
\phi(\mu) &= \rho_k J_1(\mu) Y_o(\sqrt{\rho_\alpha}\mu) - \sqrt{\rho_\alpha} J_o(\mu) Y_1(\sqrt{\rho_\alpha}\mu) \\
\psi(\mu) &= \rho_k J_1(\mu) J_o(\sqrt{\rho_\alpha}\mu) - \sqrt{\rho_\alpha} J_o(\mu) J_1(\sqrt{\rho_\alpha}\mu)
\end{aligned} \tag{21}$$

Evaluation of the interface temperature, $T_i = T_1(R_o, t) = T_2(R_o, t)$, using these expressions reveals that, in the temperature and pressure ranges of interest and for the shock-tube geometry under consideration, the value does not differ from that given by the 1-D endwall interface temperature given by Eq. 19 for times up to at least 10 ms, moreover, the thermal penetration depth in the solid sidewall obtained from Eq. 20 never reaches the outer sidewall radius within the duration of the tests, i.e. up to 20 ms, for the conditions and wall thickness of interest herein. As shown in the main body of the paper, the worst-case thermal penetration into the steel walls is less than 2 mm after 20 ms.

As such, a simpler model for the radial temperature distribution can be adopted for computations, namely, that of a cylinder imposed with constant wall temperature, T_i, whose value is given by Eq. 19. The radial temperature distribution of the test gas is then,

$$T_1(r,t) = T_i + 2(T_g - T_i)\sum_{n=1}^{\infty} \frac{J_o(\lambda_n r)}{(\lambda_n R_o) J_1(\lambda_n R_o)} e^{-\alpha_1 \lambda_n^2 t} \tag{22}$$

where J_o and J_1 are the Bessel functions of the first kind of zero and first order, respectively, and the eigenvalues λ_n are the zeroes of J_o divided by R_o.

References

1. Amadio, A.D., Crofton, M.W., Petersen, E.L.: Test-time extension behind reflected shock waves using CO_2-He and C_3H_8-He driver mixtures. Shock Waves **16**, 157–165 (2006)
2. de Vries, J., Petersen, E.L.: Autoignition of methane-based fuel blends under gas turbine conditions. Proc. Combust. Inst. **31**, 3163–3171 (2007)
3. Davidson, D.F., Hanson, R.K.: Recent advances in shock tube/laser diagnostic methods for improved chemical kinetics measurements. Shock Waves **19**, 271–283 (2009)
4. Hong, Z., Pang, G.A., Vasu, S.S., Davidson, D.F., Hanson, R.K.: The use of driver inserts to reduce non-ideal pressure variations behind reflected shock waves. Shock Waves **19**, 113–123 (2009)
5. Hong, Z., Davidson, D.F., Hanson, R.K.: Contact surface tailoring condition for shock tubes with different driver and driven section diameters. Shock Waves **19**, 331–336 (2009)
6. Bromberg, R.: Use of the shock tube wall boundary layer in heat transfer studies. Jet Propuls. **26**, 737–740 (1956)
7. Hartunian, R.A., Russo, A.L., Marrone, P.V.: Boundary-layer transition and heat transfer in shock tubes. J. Aerosp. Sci. **27**, 587–594 (1960)
8. Mirels, H.: Laminar boundary layer behind shock advancing into stationary fluid. NACA TN 3401 (1955)
9. Mirels, H.: Boundary layer behind shock or thin expansion wave moving into stationary fluid. NACA TN 3712 (1956)
10. Wilson, G.J., Sharma, S.P., Gillespie, W.D.: Time-dependent simulation of reflected-shock/boundary layer interaction in shock tubes. In: Brun, R., Dumitrescu, L.Z. (eds.) Shock Waves @Marseille I-Proceedings of the 19th International Symposium on Shock Waves, pp. 439–444. Springer, Berlin (1995)
11. Nishida, M., Lee, M.G.: Reflected shock side boundary layer interaction in a shock tube. In: Hornung, H.G., Shepherd, J.E., Sturtevant, B. (eds.), Proceedings of the 20th International Symposium on Shock Waves, vol. I, pp. 705–710. World Scientific, New York (1996)
12. Goldsworthy, F.A.: The structure of a contact region, with application to the reflexion of a shock from a heat-conducting wall. J. Fluid Mech. **5**, 164–176 (1959)
13. Sturtevant, B., Slachmuylders, E.: End-wall heat-transfer studies on the trajectory of a reflected shock wave. Phys. Fluids **7**, 1201–1207 (1964)
14. Baganoff, D.: Experiments on the wall-pressure history in shock-reflexion processes. J. Fluid Mech. **23**, 209–228 (1965)
15. Hanson, R.K.: Study of gas-solid interaction using shock-wave reflection. In: Stollery, J.L., Gaydon, A.G., Owen, P.R. (Eds.),

Shock Tube Research-Proceedings of the Eighth International Shock Tube Symposium, paper 58. Chapman and Hall, London (1971)
16. Eckert, E.M., Drake, R.: Analysis of Heat and Mass Transfer. McGraw-Hill, New York (1972)
17. Luikov, A.V.: Analytical Heat Diffusion Theory. Academic Press, New York (1968)
18. Petersen, E.L., Rickard, M.J.A., Crofton, M.W., Abbey, E.D., Traum, M.J., Kalitan, D.M.: A facility for gas- and condensed-phase measurements behind shock waves. Meas. Sci. Tech. **16**, 1716–1729 (2005)
19. White, F.M.: Viscous Fluid Flow. 2nd edn. McGraw-Hill, New York (1991)
20. Key, R.J., Rupley, F.M., Miller, J.A., Coltrin, M.E., Grcar, J.F., Meeks, E., Moffat, H.K., Lutz, A.E., Dixon-Lewis, G., Smooke, M.D., Warnatz, J., Evans, G.H., Larson, R.S., Mitchell, R.E., Petzold, L.R., Reynolds, W.C., Caracotsios, M., Stewart, W.E., Glarborg, P., Wang, C., Adigun, O.: Chemkin Collection, Release 3.6. Reaction Design, San Diego (2000)
21. Driscoll, J.F., Khatib-Shahidi, B., Liu, T., Nicholls, J.A., Patel, V.: Shock tube study of the ignition and combustion of aluminum. AIAA Paper 84-1201 (1984)
22. Teshima, K., Deguchi, M., Takahashi, N.: Thermal boundary layer effects on mass sampling from a shock tube. Jpn. J. Appl. Phys. **23**, 118–123 (1984)
23. Lamnaouer, M., Kassab A.J., Divo E., Petersen E.L.: Time accurate simulations of shock propagation and reflection in an axisymmetric shock tube. AIAA Paper 2010-0926 (2010)
24. de Vries, J., Aul, C., Barrett, A., Lambe, D., Petersen, E.L.: Shock-tube development for high-pressure and low-temperature chemical kinetics experiments. In: Hannemann, K., Seiler, F. (eds.), Shock Waves: 26th International Symposium on Shock Waves pp. 171–176. Springer, Berlin (2009)